Identifiability of Lithium-Ion Battery Electrolyte Dynamics*

Luis D. Couto[1], Ross Drummond[2], Dong Zhang[3], Toby Kirk[4] and David A. Howey[2,5]

***Abstract*— The growing need for improved battery fast charging algorithms and management systems is pushing forward the development of high-fidelity electrochemical models of cells. Critical to the accuracy of these models is their parameterisation, however this challenge remains unresolved, both in terms of theoretical analysis and practical implementation. This paper develops a framework to analyse from impedance measurements the identifiability of electrolyte dynamics—a subcomponent of a general Li-ion model that is key to enabling accurate fast charging simulations. By assuming that the electrolyte volume fractions in the electrode and separator regions are equal, an analytic expression for the impedance function of the electrolyte dynamics is obtained, and this can be tested for structural identifiability. It is shown that the only parameters of the electrolyte model that may be identified are the diffusion time scale and a geometric coupling parameter. Simulations highlight the identifiability issues of electrolyte dynamics (relating to symmetric cells) and explain how the electrolyte parameters might be identified.**

I. INTRODUCTION

Within the last decade, Li-ion batteries have emerged as the dominant solution for electrical energy storage and are now near omnipresent and encountered on a daily, even hourly, basis. The range of applications for Li-ion batteries is growing and includes providing electricity storage for renewable energy integration within the grid and powering electric vehicles, where high energy density, increased power per unit mass [1] and declining costs have made them the preferred power sources for transport electrification. Demanding activities such as these require a battery management systems (BMS) to monitor internal states to mitigate safety risks and increase lifetime [1], with the states of the battery typically estimated using a model.

Several types of battery model have been developed for different purposes. The simplest are those where the dynamics are based upon equivalent circuits [2], where the electrical analogy of a battery is exploited. Although a reasonable voltage prediction can be obtained with this framework, it suffers from the fact that its internal battery states have only faint connections to reality. In order to capture physical battery behaviour that might then be tracked by next generation BMSs, electrochemical models are useful. Of these, the Doyle-Fuller-Newman (DFN) model [3] is now regarded as a benchmark and is widely used within academia and industry. However, this model is computationally demanding and has many parameters, and this has restricted its use within BMS and for other practically relevant applications. To reduce this complexity whilst still retaining some of the physical usefulness of the DFN model, several reduced-order electrochemical models have been developed.

The most popular reduced-order electrochemical battery model is perhaps the "single-particle model" (SPM) [4], [5] which assumes that the cell experiences a uniform spatial electrochemical reaction rate and a constant electrolyte concentration profile across its thickness. These assumptions allow the battery to be idealised as a single spherical average particle per electrode whose surface area density is scaled to that of the porous electrode [5]. Although the SPM has been shown to be computationally simple and physically relevant, it has limitations e.g. it only provides accurate predictions for relatively low C-rates [6]. However, the value of electrochemical information will be of most significance for high rate operations, since it is when the battery is acting near its performance limits that detailed monitoring is most valuable. One way to increase the applicability of the SPM is to add more dynamics to it that are relevant at higher C-rates, notably those for the transport of ions within the bulk electrolyte, and this results in the "SPM with electrolyte dynamics" (SPMe) model [7], [8], [9], [10], [6], [11].

Even though these electrochemical models are widely used, it is becoming increasingly apparent that the validity of their state predictions is strongly dependent upon the accuracy of their parameters, and yet we still have very limited tools for battery model parameter estimation. While it is widely acknowledged that parameter estimation is an integral part of the modeling effort, most studies have tended to avoid the burden of identification and instead obtained the model parameters directly from literature. Whilst enabling quick model-to-model comparison, the limitations of this are i) the parameters might differ from the real parameters of the specific cell under study, especially as the cells age, and ii) the release of new battery chemistries is happening at a faster rate than cell models are being parameterised, leading to a parameterisation backlog. For these reasons, *in situ* determination of cell properties from simple non-invasive measurements is required for practical applications of electrochemical models. However, determining parameter values is hard and requires both time, resources and a range

*L.D. Couto would like to thank the Wiener-Anspach Foundation for its financial support. This work was supported by the Fond de la Recherche Scientifique - FNRS under grant n°T.0142.20

[1]L.D. Couto (lcoutome@ulb.ac.be) is with with the School of Engineering of the Université Libre de Bruxelles, B-1050 Brussels, Belgium.

[2]R. Drummond (ross.drummond@eng.ox.ac.uk) and D.A. Howey (david.howey@eng.ox.ac.uk) are with the Department of Engineering Science, University of Oxford, Oxford OX1 3PJ, UK.

[3]D. Zhang (dzhang@ou.edu) is with School of Aerospace and Mechanical Engineering, The University of Oklahoma, Norman, OK, USA.

[4]T. Kirk (toby.kirk@maths.ox.ac.uk) is with the Mathematical Institute, University of Oxford, Oxford OX2 6GG, UK.

[5]D.A. Howey is also with the Faraday Institution, Harwell Campus, Didcot, OX11 0RA, UK.

of experimental techniques [7].

To support these efforts, this paper develops a structural identifiability analysis of the electrolyte sub-model of the SPMe by analysing the electrolyte's impedance function as might be measureable from, e.g., electrochemical impedance spectroscopy (EIS). In the language of control theory, the impedance function is the transfer function which is known to contain information about kinetic and transport parameters and can also be used to study reaction mechanisms and degradation effects [12]. The usefulness of battery model parameterisation from EIS data has motivated several existing studies on this problem, including [13] and [14], which we extend in this paper in the following ways:

- An impedance model for the electrolyte dynamics is derived;
- The resulting electrolyte impedance model is analyzed under different conditions;
- The associated identifiability properties are studied, and a possible strategy to improve identifiability is proposed.

By developing the theory of what is achievable for electrochemical battery model parameterisation, it is hoped that this work will eventually contribute to enabling more effective practical tools to increase model accuracy, enabling the models to be tuned online to improve BMS operation, fast charging algorithms and state-of-health predictors.

II. ELECTROLYTE DYNAMICS

In this section, a frequency-domain model of electrolyte dynamics is considered. We first introduce electrolyte-phase model equations, followed by the voltage measurement equation and the impedance model.

A. Electrolyte-phase model

In contrast to the solid-phase model for battery electrodes whose transcendental transfer functions have been reported in several papers (see e.g. [15]), the derivation of the transfer functions associated with the electrolyte-phase model is more scarce.

The electrolyte-phase dynamics in a lithium-ion battery are described by the following partial-differential equation (PDE) system [3],

$$\frac{\partial c_e^-}{\partial t}(x,t) = \frac{D_{e,\text{eff}}^-}{\varepsilon_e^-}\frac{\partial^2 c_e^-}{\partial x^2}(x,t) + \frac{1-t_c^0}{\varepsilon_e^-}a_s^- j_n^-(x,t) \quad (1)$$

$$\frac{\partial c_e^s}{\partial t}(x,t) = \frac{D_{e,\text{eff}}^s}{\varepsilon_e^s}\frac{\partial^2 c_e^s}{\partial x^2}(x,t) \quad (2)$$

$$\frac{\partial c_e^+}{\partial t}(x,t) = \frac{D_{e,\text{eff}}^+}{\varepsilon_e^+}\frac{\partial^2 c_e^+}{\partial x^2}(x,t) + \frac{1-t_c^0}{\varepsilon_e^+}a_s^+ j_n^+(x,t), \quad (3)$$

where $c_e(x,t)$ and $j_n(x,t)$ are the molar electrolyte concentration per unit volume of electrode and the pore-wall molar flux, respectively, x and t stand for the longitudinal direction along the cell thickness and the temporal dimension, respectively, and superscripts $\{+,s,-\}$ indicate positive electrode, separator and negative electrode domains, respectively. The effective electrolyte diffusion coefficient $D_{e,\text{eff}}$ has the form $D_{e,\text{eff}}^{\pm s} = D_e(\varepsilon_e^{\pm s})^b$ where the shorthand notation "$\pm s$" in superscript denotes positive electrode $(+)$, negative electrode $(-)$ and separator (s), ε_e is the electrolyte volume fraction and b is the Bruggeman's exponent. The transference number is denoted as t_c^0. The PDE system (1)-(3) is subject to the following boundary conditions,

$$\left.\frac{\partial c_e^-}{\partial x}(x,t)\right|_{x=0} = \left.\frac{\partial c_e^+}{\partial x}(x,t)\right|_{x=L} = 0 \quad (4)$$

$$\left. D_{e,\text{eff}}^- \frac{\partial c_e^-}{\partial x}(x,t)\right|_{x=L_n} = \left. D_{e,\text{eff}}^s \frac{\partial c_e^s}{\partial x}(x,t)\right|_{x=L_n} \quad (5)$$

$$\left. D_{e,\text{eff}}^s \frac{\partial c_e^s}{\partial x}(x,t)\right|_{x=L_{ns}} = \left. D_{e,\text{eff}}^+ \frac{\partial c_e^+}{\partial x}(x,t)\right|_{x=L_{ns}} \quad (6)$$

$$c_e^-(x,t)\big|_{x=L_n} = c_e^s(x,t)|_{x=L_n} \quad (7)$$

$$c_e^s(x,t)|_{x=L_{ns}} = c_e^+(x,t)\big|_{x=L_{ns}}, \quad (8)$$

for a battery cell whose thicknesses for negative electrode, separator and positive electrode are denoted as L_n, L_s and L_p respectively, $L = L_n + L_s + L_p$ and $L_{ns} = L_n + L_s$.

The pore-wall molar flux in (1)-(3) can be simplified by assuming a uniform reaction across the electrode thickness, which is a typical reduction of SPM-type models, given by

$$j_n^{\pm}(x,t) \approx \mp \frac{i(t)}{a_s^{\pm} F L^{\pm} A} \quad (9)$$

where $i(t)$ is the applied battery current, a_s is the specific interfacial area, F is Faraday's constant, L is the electrode thickness and A is the transverse cell area. Moreover, we can normalise the model equations by defining $c_e^* = c_e/c_{e,\text{m}}$ and $i^* = i/i_{\text{typ}}$ where $c_{e,\text{m}}$ and i_{typ} are a nominal electrolyte concentration and current, respectively. Let us define the following grouped parameters

$$\tau_{e,c}^{\pm} = \frac{\varepsilon_e^{\pm} F A L^{\pm} c_{e,\text{m}}}{(1-t_c^0) i_{\text{typ}}}, \quad \alpha^{\pm s} = D_e\left(\varepsilon_e^{\pm s}\right)^{b-1}. \quad (10)$$

By taking the Laplace transform of (1)-(3) normalised by $c_{e,m}$, the following ordinary-differential equation system in the frequency domain is obtained

$$sC_e^{-,*}(x,s) = \alpha^- \frac{\mathrm{d}^2 C_e^{-,*}}{\mathrm{d}x^2}(x,s) + \frac{1}{\tau_{e,c}^-} I^*(s) \quad (11)$$

$$sC_e^{s,*}(x,s) = \alpha^s \frac{\mathrm{d}^2 C_e^{s,*}}{\mathrm{d}x^2}(x,s) \quad (12)$$

$$sC_e^{+,*}(x,s) = \alpha^+ \frac{\mathrm{d}^2 C_e^{+,*}}{\mathrm{d}x^2}(x,s) - \frac{1}{\tau_{e,c}^+} I^*(s), \quad (13)$$

where s is the Laplace variable and $C_e^*(s)$ and $I^*(s)$ are the transforms of the normalised electrolyte-phase lithium concentration c_e^* and current i^*, respectively.

The general solutions of (11)-(13) are given by

$$C_e^{-,*}(x,s) = K_1 \exp\left(\beta^- x\right) + K_2 \exp\left(-\beta^- x\right) + \frac{1}{\tau_{e,c}^- s} I^*(s) \quad (14)$$

$$C_e^{s,*}(x,s) = K_3 \exp\left(\beta^s x\right) + K_4 \exp\left(-\beta^s x\right) \quad (15)$$

$$C_e^{+,*}(x,s) = K_5 \exp\left(\beta^+ x\right) + K_6 \exp\left(-\beta^+ x\right) - \frac{1}{\tau_{e,c}^+ s} I^*(s) \quad (16)$$

where $\beta^{\pm s} = \sqrt{s/\alpha^{\pm s}}$ and K_i, $i = 1,\ldots,6$ are unknown constants. These constants are obtained by substituting (14)-(16) into the normalised version of the boundary conditions (4)-(8) and solving the resulting set of six algebraic

equations. Doing so gives an algebraic characterisation (see Appendix) of the impedance function, expressed in terms of parameters such as diffusion coefficients, electrodes thicknesses, etc.

Inspecting the algebraic characterisation of the electrolyte impedance given in (A.1) of the Appendix, it is apparent that this expression is both long and convoluted, with many (at least 10) parameters, including $\tau_{e,c}^{\pm}$, $\tau_{ed}^{-,n}$, $\tau_{ed}^{s,n}$, $\tau_{ed}^{s,ns}$, $\tau_{ed}^{+,ns}$, τ_{ed}^{+} (defined in Table I), and $D_{e,\text{eff}}^{\pm s}/L^2$, with no trivial parameter groupings. The non-existence of a clean, relatively simple and preferably analytical (for tractability) expression for the coefficients $K_{1:6}$ complicates the goal of this paper which is to investigate the structural identifiability of these electrolyte dynamics. Therefore in the following subsection we describe two different forms that these local electrode impedances can take, based upon two simplifying assumptions on the electrode microstructure.

B. Electrolyte model simplification

To simplify the impedance expressions, the following assumption is applied:

(A1) The volume fraction of the electrolyte phase ε_e is uniform throughout electrolyte regions, i.e. $\varepsilon_e = \varepsilon_e^- = \varepsilon_e^s = \varepsilon_e^+$, which implies a uniform effective diffusion coefficient $D_{e,\text{eff}} = D_e \varepsilon_e^b$ and therefore $\beta = \sqrt{s/\alpha}$.

Note that since the volume fraction is bounded by $\varepsilon_e^{\{+,-,s\}} \in [0,1]$ and typically only differs by ≈ 0.2 between each domain, this assumption is generally not too restrictive. Applying Assumption (A1) greatly simplifies the problem, giving a compact analytic expression for the impedance model for each electrolyte region.

Defining the electrolyte-phase diffusion timescales

$$\tau_{e,d}^j = \frac{\beta^2}{s} L_j^2 = \frac{L_j^2}{D_e \varepsilon_e^{b-1}}, \tag{17}$$

with $j = \{n, ns, \cdot\}$ attributed to L_n, L_{ns} and L, respectively, the following parameterised transfer functions for the normalised electrolyte concentration in the negative and positive battery terminals are obtained:

$$H_e^{0,*}(s, \boldsymbol{\theta_e}) = \frac{1}{\tau_{e,c}^- s} - \frac{\frac{1}{\tau_{e,c}^-}\sinh\left(\sqrt{\tau_{e,d}\, s} - \sqrt{\tau_{e,d}^n\, s}\right) + \frac{1}{\tau_{e,c}^+}\sinh\left(\sqrt{\tau_{e,d}\, s} - \sqrt{\tau_{e,d}^{ns}\, s}\right)}{s \sinh\left(\sqrt{\tau_{e,d}\, s}\right)} \tag{18}$$

$$H_e^{L,*}(s, \boldsymbol{\theta_e}) = -\frac{1}{\tau_{e,c}^+ s} + \frac{\frac{1}{\tau_{e,c}^-}\sinh\left(\sqrt{\tau_{e,d}^n\, s}\right) + \frac{1}{\tau_{e,c}^+}\sinh\left(\sqrt{\tau_{e,d}^{ns}\, s}\right)}{s \sinh\left(\sqrt{\tau_{e,d}\, s}\right)} \tag{19}$$

Here, $H_e^{\{0,L\},*}(s, \boldsymbol{\theta_e}) = C_e^{\{0,L\},*}(s)/I^*(s)$ where $C_e^{0,*}(s) = C_e^{-,*}(0,s)$ and $C_e^{L,*}(s) = C_e^{+,*}(L,s)$. The transfer functions $H_e^{\{0,L\},*}(s, \boldsymbol{\theta_e})$ in (18),(19) can be parameterised by $\boldsymbol{\theta_e} = [\tau_{e,d} \;\; \tau_{e,d}^n \;\; \tau_{e,d}^{ns} \;\; \tau_{e,c}^- \;\; \tau_{e,c}^+]^\top$.

Remark 1: Assume that

(A2) The proportions of electrolyte regions $\delta_n = L_n/L$ and $\delta_{ns} = L_{ns}/L$ are known,

TABLE I

GROUPED PARAMETERS OF THE ELECTROLYTE MODEL

Parameter	Symbol
Geometric coupling parameter in negative electrode	$\tau_{e,c}^-$
Geometric coupling parameter in positive electrode	$\tau_{e,c}^+$
Diffusion timescale in negative electrode at L_n	$\tau_{e,d}^{-,n}$
Diffusion timescale in separator at L_n	$\tau_{e,d}^{s,n}$
Diffusion timescale in separator at L_{ns}	$\tau_{e,d}^{s,ns}$
Diffusion timescale in positive electrode at L_{ns}	$\tau_{e,d}^{+,ns}$
Diffusion timescale in positive electrode at L	$\tau_{e,d}^{+}$

then the electrolyte diffusion timescales in (17) can be written in terms of the total cell thickness L, i.e. $\tau_{e,d}^n = \delta_n^2 \tau_{e,d}$ and $\tau_{e,d}^{ns} = \delta_{ns}^2 \tau_{e,d}$. Under this further simplification, the impedances in (18), (19) become

$$\hat{H}_e^{0,*}(s, \boldsymbol{\theta_{e,3}}) = \frac{1}{\tau_{e,c}^- s} - \frac{\frac{1}{\tau_{e,c}^-}\sinh\left((1-\delta_n)\sqrt{\tau_{e,d}\, s}\right) + \frac{1}{\tau_{e,c}^+}\sinh\left((1-\delta_{ns})\sqrt{\tau_{e,d}\, s}\right)}{s \sinh\left(\sqrt{\tau_{e,d}\, s}\right)} \tag{20}$$

$$\hat{H}_e^{L,*}(s, \boldsymbol{\theta_{e,3}}) = \frac{-1}{\tau_{e,c}^+ s} + \frac{\frac{1}{\tau_{e,c}^-}\sinh\left(\delta_n\sqrt{\tau_{e,d}\, s}\right) + \frac{1}{\tau_{e,c}^+}\sinh\left(\delta_{ns}\sqrt{\tau_{e,d}\, s}\right)}{s \sinh\left(\sqrt{\tau_{e,d}\, s}\right)} \tag{21}$$

and these are characterised by 3 parameters, namely $\boldsymbol{\theta_{e,3}} = [\tau_{e,d} \;\; \tau_{e,c}^- \;\; \tau_{e,c}^+]^\top$. In this case, the relationship $\tau_{e,c}^-/\tau_{e,c}^+ = \delta_n/(1-\delta_{ns})$ holds, which means that δ_n can be written in terms of the other parameters.

Remark 2: Impedances (20), (21) can be simplified even further if it is assumed that

(A3) A geometrically symmetric cell is considered, meaning that the electrode thicknesses are equivalent, namely $L_n = L_p$.

In this case, $\tau_{e,c} = \tau_{e,c}^- = \tau_{e,c}^+$ and the models reduce to

$$\bar{H}_e^{0,*}(s, \boldsymbol{\theta_{e,2}}) = \frac{1}{\tau_{e,c}}\left(\frac{1}{s} - \frac{\sinh\left(\bar{\delta}_n\sqrt{\tau_{e,d}\, s}\right) + \sinh\left(\bar{\delta}_{ns}\sqrt{\tau_{e,d}\, s}\right)}{s \sinh\left(\sqrt{\tau_{e,d}\, s}\right)}\right) \tag{22}$$

$$\bar{H}_e^{L,*}(s, \boldsymbol{\theta_{e,2}}) = -\frac{1}{\tau_{e,c}}\left(\frac{1}{s} - \frac{\sinh\left(\delta_n\sqrt{\tau_{e,d}\, s}\right) + \sinh\left(\delta_{ns}\sqrt{\tau_{e,d}\, s}\right)}{s \sinh\left(\sqrt{\tau_{e,d}\, s}\right)}\right) \tag{23}$$

with $\bar{\delta}_{\{n,ns\}} = 1 - \delta_{\{n,ns\}}$ and which are characterised by 2 parameters, $\boldsymbol{\theta_{e,2}} = [\tau_{e,d} \;\; \tau_{e,c}]^\top$.

C. Voltage drop from the bulk electrolyte

Recall that impedance requires one to know the mapping from the applied current to the measured voltage drop. In terms of the electrolyte contribution, the voltage drop is related to the difference in the electrolyte concentrations at either current collector, described by

$$v^*(t) = k_c\left(\ln(c_e^{L,*}(t)) - \ln(c_e^{0,*}(t))\right) + Ri^*(t) \tag{24}$$

with resistance

$$R = \frac{(L_n + 2L_s + L_p) i_{\text{typ}}}{2\kappa A \mu} \tag{25}$$

and where the non-dimensional voltage v^* is defined as $v^* = v/\mu$, v is the dimensional voltage and $\mu = R_g T_{\text{ref}}/(\alpha_0 F)$ is the thermal potential with R_g the universal gas constant, T_{ref} a reference temperature and α_0 the charge transfer

coefficient. The ionic conductivity is denoted as κ, $k_c = 2\alpha_0(1-t_c^0)(1+d\ln f_{c/a}/d\ln c_e)$ and $f_{c/a}$ is the activity coefficient.

In the following, it will be assumed that the contributions to the measured voltage drop from the bulk electrolyte (described above) are essentially decoupled from those of the active particles and kinetics. Such an assumption is immediate at the points when the open-circuit potential function of the electrodes is flat versus the state-of-charge, as can occur with LFP or LTO cells, but can also follow from the fact that there is a timescale separation between Li diffusion in the particles ($\approx 10^3$ s), bulk electrolyte (≈ 10 s) and double layer ($\approx 10^{-3}$ s), with this separation meaning that the relevant frequencies where these three phenomena are dominant are somewhat disjoint

Assuming that the current magnitude $i(t)$ is small and the battery is operated close to a given initial equilibrium condition $c_e^{\{0,L\},*}$, the voltage equation can be linearized using a first-order Taylor series approximation about the reference point $\mathrm{z}_0^* = [c_{e,0}^{0,*} \;\; c_{e,0}^{L,*} \;\; i_0^*]^\top = 0$ resulting in

$$\tilde{v}^*(t) \approx \left.\frac{\partial v^*}{\partial c_e^{0,*}}\right|_{\mathrm{z}_0^*} \tilde{c}_e^{0,*}(t) + \left.\frac{\partial v^*}{\partial c_e^{L,*}}\right|_{\mathrm{z}_0^*} \tilde{c}_e^{L,*}(t) + \left.\frac{\partial v^*}{\partial i^*}\right|_{\mathrm{z}_0^*} \tilde{i}^*(t) \tag{26}$$

where notation such as $\tilde{v}^* = v^* - v_0^*$ for voltage denotes the difference between a given variable v^* and the equilibrium point v_0^* (similarly for $c_e^{\{0,L\},*}$ and i^*).

The first two terms in the right-hand-side (RHS) of (26) take the form

$$\left.\frac{\partial v^*}{\partial c_e^{0,*}}\right|_{\mathrm{z}_0^*} = -k_c \frac{1}{c_{e,0}^{0,*}}, \quad \left.\frac{\partial v^*}{\partial c_e^{L,*}}\right|_{\mathrm{z}_0^*} = k_c \frac{1}{c_{e,0}^{L,*}}, \tag{27}$$

and the last term in the RHS of (26) is

$$\left.\frac{\partial v^*}{\partial i^*}\right|_{\mathrm{z}_0^*} = \frac{(L_n + 2L_s + L_p) i_{\mathrm{typ}}}{2\kappa A \mu} = R. \tag{28}$$

For the sake of simplicity, this work assumes that the parameter R in (26)-(28) can be estimated independently of the other parameters [13] and is therefore ignored in the rest of this analysis. Taking the Laplace transform of the linearized voltage equation (26)-(28) and dividing by the current $I^*(s)$ yields the transfer function $H_v^*(s,\boldsymbol{\theta}) = \tilde{V}^*(s)/I^*(s)$ about the equilibrium point $\mathrm{z}_0^* = [c_{e,0}^{0,*} \;\; c_{e,0}^{L,*} \;\; i_0^*]^\top = 0$ given by

$$H_v^*(s,\boldsymbol{\theta}) = \frac{k_c}{c_{e,L}^*} \check{H}_e^{L,*}(s,\boldsymbol{\theta}) - \frac{k_c}{c_{e,0}^*} \check{H}_e^{0,*}(s,\boldsymbol{\theta}) \tag{29}$$

In this work, the transfer functions $\check{H}_e^{\{0,L\},*}$ take the reduced-order form of (20), (21) when the model in Remark 1 is considered (i.e. $\check{H}_e^{\{0,L\},*} = \hat{H}_e^{\{0,L\},*}$ and $\boldsymbol{\theta} = \boldsymbol{\theta_{e,3}}$), and the form of (22),(23) when the form of Remark 2 is used (i.e. $\check{H}_e^{\{0,L\},*} = \bar{H}_e^{\{0,L\},*}$ and $\boldsymbol{\theta} = \boldsymbol{\theta_{e,2}}$). Note that in (29) the parameter k_c is required to be known. However, if it is not known, the analysis is unchanged since k_c can be grouped with $\tau_{e,c}^{\pm}$ in the transfer functions $\check{H}_e^{\{0,L\},*}$ to form a new unknown lumped parameter.

III. MODEL IDENTIFICATION

In order to estimate the parameters of the electrolyte impedance model in (29), we first verify its structural identifiability and then propose a cost function for parameter identification.

A. Structural identifiability

The identifiability properties of the considered system are assessed through structural identifiability [16], [17].

Definition 1 (Structural identifiability): Consider a model structure $\mathcal{M}$ with the transfer function $H(s,\boldsymbol{\theta})$ parameterised by $\boldsymbol{\theta} \subset \mathbb{R}^n$ where n denotes the number of parameters of the model. The identifiability equation for $\mathcal{M}$ is given by:

$$H(s,\boldsymbol{\theta}) = H(s,\boldsymbol{\theta}') \text{ for almost all } s \tag{30}$$

where $\boldsymbol{\theta}, \boldsymbol{\theta}' \in \mathcal{D}$. The model structure $\mathcal{M}$ is said to be

- globally identifiable if (30) has a unique solution in $\mathcal{D}$,
- locally identifiable if (30) has a finite number of solutions in $\mathcal{D}$,
- unidentifiable if (30) has a infinite number of solutions in $\mathcal{D}$.

A globally identifiable model is said to be structurally identifiable and the parameter estimation problem in theory admits a unique solution. Once structural identifiability is verified for a given number of parameters, then the model parameters can be estimated from data.

B. Frequency-domain parameter estimation

The measured impedance of a cell at a given frequency ω_i is given by the complex number $Z(\omega_i) = Z'(\omega_i) + \mathrm{i}Z''(\omega_i)$, where Z' and Z'' denote the real and imaginary part respectively. The optimal parameter estimate can be obtained by solving the following optimization problem [13]

$$\min_{\boldsymbol{\theta}} \;\; J(\boldsymbol{\theta}) = \min_{\boldsymbol{\theta}} \;\; \sum_{i=1}^{N_\omega} |Z(\omega_i) - H(\omega_i,\boldsymbol{\theta})|^2 \tag{31}$$

where N_ω is the number of evaluated frequencies. This cost function is used below to create the estimation error surface for two parameters varying simultaneously, with the minimum corresponding to the best parameter fit.

IV. RESULTS AND DISCUSSION

Simulations are now developed to evaluate the identifiability issues highlighted in the previous sections. In the following, we first analyze the electrolyte impedance model in terms of frequency response then study the identifiability properties of the model by estimating the model parameters.

A. Model analysis

Let us first consider the simplest models $\bar{H}_e^{\{0,L\},*}(s,\boldsymbol{\theta_{e,2}})$ with 2 parameters, as stated in Remark 2, given by (22),(23). Note that the lumped parameters $\{\tau_{e,d}, \tau_{e,c}\}$ are mapped to the physical parameters $\{L_n, \varepsilon_e\}$ and we make the latter vary. Fig. 1a shows the Nyquist plots of the electrolyte impedance at $x = L$ for different values of electrode thickness L_n (lowest value as solid blue curve and increasing up to highest

value as solid red curve). The same figure also shows the frequency response at $x = 0$ with the lowest value as a dashed magenta curve and the highest value as a dashed cyan curve[1]. From the figure, it follows that the electrolyte system exhibits a response similar to an RC pair characterised by a semi-circle [18], [19]. This is interesting since the transfer functions in (22),(23) appear at first glance to have a pole at $s = 0$ (i.e. $\omega = 0$), but this does not appear in the Nyquist plot. This is due to the fact that the pole at the origin is canceled by a pole from the second term of the expression. To see this, take the Laurent series expansion of (22) or (23) around $s = 0$,

$$\bar{H}_e^{\{0,L\},*}(s, \boldsymbol{\theta_{e,2}}) = \frac{1 - \delta_n - \delta_{ns}}{\tau_{e,c}\ s} + \cdots$$

For a symmetric cell model, $\delta_n = \delta_p$ and therefore $\delta_n + \delta_{ns} = 1$, which explains the disappearance of the pole at the origin for the electrolyte concentration in an electrode domain.

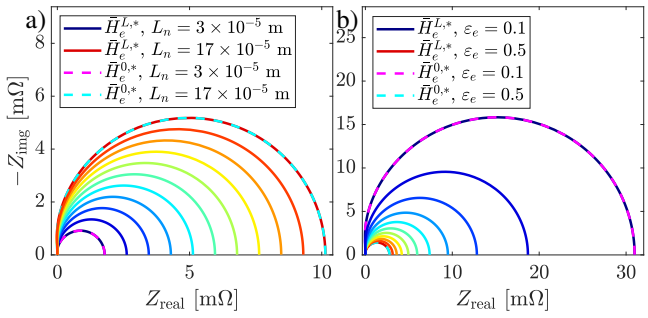

Fig. 1. Nyquist plots of electrolyte impedance response for 2-parameters model $\bar{H}_e^{\{0,L\},*}(s, \boldsymbol{\theta_{e,2}})$ with frequency range of 2 μHz to 160 kHz considering a) constant ε_e and b) constant L_n.

The same method of Fig. 1a was used to build Fig. 1b but with the electrolyte volume fraction ε_e varying. Similar results in terms of $x = \{0, L\}$ symmetry and RC-pair behaviour can be seen in that figure, but the main difference with respect to the thickness parameter is that the increase in the volume fraction ε_e reduces the impedance response (smaller semi-circles from solid blue curves to solid red curves). Larger volume fractions for the electrolyte can be practically seen as a result of having more electrolyte volume in the battery, which effectively reduces the associated impedance.

To evaluate the differences between the simpler and more complex models, we performed a similar study as before but with the model $\hat{H}_e^{\{0,L\},*}(s, \boldsymbol{\theta_{e,3}})$ with 3 parameters, as stated in Remark 1 and given by (20), (21). Similarly as before, the lumped parameters $\{\tau_{e,d}, \tau_{e,c}\}$ are mapped to the physical parameters $\{L_n, \varepsilon_e\}$ and we make the latter vary. The obtained results are shown in Fig. 2a for variations in L_n, where it can be seen that the semi-circle impedance response is preserved. Again, consideration of the Laurent series expansion of (20), (21) around $s = 0$ results in

$$\hat{H}_e^{\{0,L\},*}(s, \boldsymbol{\theta_{e,3}}) = \pm \frac{(\tau_{e,c}^{+})^{-1}(\delta_{ns} - 1) + (\tau_{e,c}^{-})^{-1}\delta_n}{s} + \cdots$$

[1]These plot conventions are used throughout this section and are only stated here to avoid repetition.

where the sign $+$ and $-$ correspond to the expression for $x = 0$ and $x = L$, respectively. Since $\delta_{ns} - 1 = -\delta_p$ and $(\tau_{e,c}^{+})^{-1} = (\tau_{e,c}^{-})^{-1}\delta_n/(1 - \delta_{ns})$, the numerator becomes zero and the pole at the origin is cancelled. Note, moreover, that the impedance again increases with larger electrode thickness. However, the symmetry is lost between the electrolyte responses, with a higher impedance for the $x = 0$ position (dashed magenta and cyan curves) than for the $x = L$ position (solid blue and red curves) given that the negative electrode volume is different than the positive electrode one ($L_n \neq L_p$).

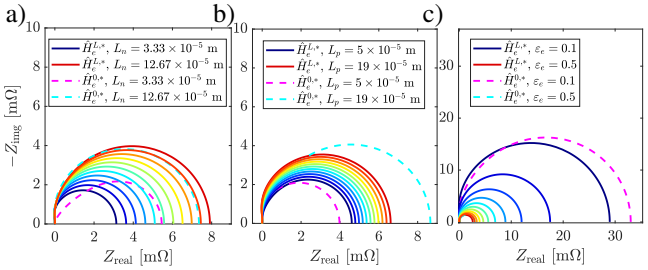

Fig. 2. Nyquist plots of electrolyte impedance response for 3-parameters model $\hat{H}_e^{\{0,L\},*}(s, \boldsymbol{\theta_{e,3}})$ with frequency range of 2 μHz to 160 kHz considering a) constant ε_e and L_p, b) constant ε_e and L_n and c) constant L_n and L_p.

Fig. 2b shows the results for changes in the positive electrode thickness L_p whereas variations in the electrolyte volume fraction ε_e are considered in Fig. 2c for constant values of L_n. In these cases, similar results are obtained: the impedance increases with larger L_p, the symmetry at $x = 0$ and $x = L$ is lost due to $L_p \neq L_n$ (Fig. 2b) and the impedance decreases for higher values of ε_e (Fig. 2c). These results reveal that, for the considered two simplified models, the frequency characteristics of the electrolyte impedance response are similar when some specific geometric parameters are manipulated. Usually the individual electrochemical parameters of a cell are numerous, and not available, and therefore parameters are often grouped in a relevant set of lumped parameters as presented in Section II (as in [13], [11], [14]), which alleviates over-parameterisation and facilitates the parameter identification process. Next, we evaluate the identification properties of both simplified models, the one with 2 parameters and the other one with 3 parameters, under the assumption that the model parameters are unknown and therefore we consider their lumped versions.

B. Parameter identification

In order to assess the identifiability properties of the proposed models, surfaces of the output error cost function (31) were built for different values of two specific parameters during each simulation. As in the previous section, we first consider the 2-parameters model $\bar{H}_e^{\{0,L\},*}(s, \boldsymbol{\theta_{e,2}})$ and evaluate $\tau_{e,c}$ and $\tau_{e,d}$. The top view of the resulting surface is shown in Fig. 3a. The red dot in the point $\tau_{e,d} = 331.55$ s and $\tau_{e,c} = 473.75$ s corresponds to the nominal parameter value used as a ground truth. The figure shows a clear valley in the cost function, indicating that multiple values of the pair $(\tau_{e,d}, \tau_{e,c})$ can minimize it which indicates structural

identifiability problems. The parameter values causing the identifiability issues can be obtained by solving (31) with respect to $\tau_{e,c}$ for given values of $\tau_{e,d}$ in $H(\omega_i, \boldsymbol{\theta})$ where $Z(\omega_i)$ is generated with nominal parameters. This is equivalent to verifying (30) numerically. The resulting $(\tau_{e,d}, \tau_{e,c})$ combination minimizing the cost (31) is also plotted in the figure as the dashed cyan curve denoted as equilibrium point 1 (eq1), since it was obtained at the nominal electrolyte concentration equilibrium point $c_{e,0} = c_{e,L} = c_{e,\text{eq}}$ in (29). From the figure it follows that the relationship between the two parameters seems to be linear, showing the possible difficulties in estimating both $\tau_{e,d}$ and $\tau_{e,c}$ simultaneously using model $\bar{H}_e^{\{0,L\},*}(s, \boldsymbol{\theta_{e,2}})$.

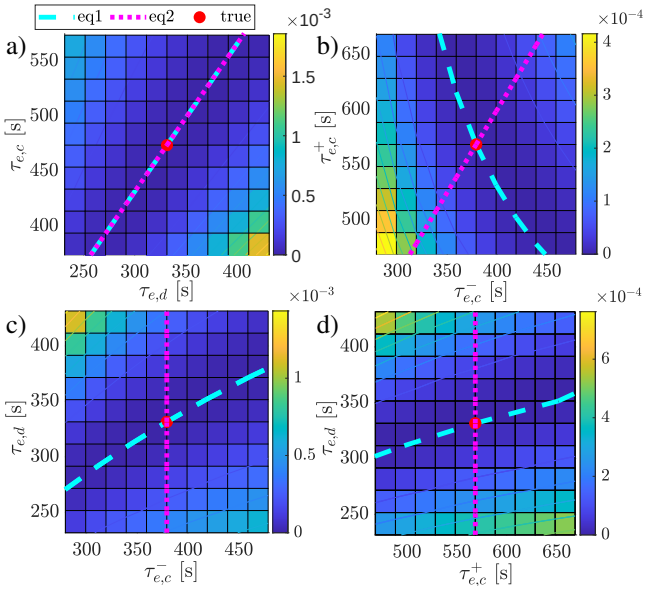

Fig. 3. Top view of the output error surfaces of electrolyte impedance response for a) 2-parameters model $\bar{H}_e^{\{0,L\},*}(s, \boldsymbol{\theta_{e,2}})$ as well as 3-parameters model $\hat{H}_e^{\{0,L\},*}(s, \boldsymbol{\theta_{e,3}})$ with varying b) $\tau_{e,c}^{\pm}$, c) $(\tau_{e,d}, \tau_{e,c}^{-})$ and d) $(\tau_{e,d}, \tau_{e,c}^{+})$. Parameter combinations that minimize the output error for each case are represented by magenta and cyan curves for equilibrium point 1 (eq1, i.e. $c_{e,0} = c_{e,L} = c_{e,\text{eq}}$) and equilibrium point 2 (eq2, i.e. $c_{e,0} = 10c_{e,\text{eq}}$, $c_{e,L} = c_{e,\text{eq}}/10$), respectively.

We now consider the model $\hat{H}_e^{\{0,L\},*}(s, \boldsymbol{\theta_{e,3}})$ and fixed the parameter $\tau_{e,d} = 331.55$ s while evaluating the parameters $\tau_{e,c}^{+}$ and $\tau_{e,c}^{-}$. The resulting top view surface is shown in Fig. 3b. Similarly as before, multiple parameter combinations $(\tau_{e,c}^{+}, \tau_{e,c}^{-})$ yield a valley in the cost function, whose minima are represented as the dashed cyan curve. In contrast to the previous model with a linear relation between $\tau_{e,d}$ and $\tau_{e,c}$, the relationship between $\tau_{e,c}^{+}$ and $\tau_{e,c}^{-}$ seems to be nonlinear.

A similar procedure can be applied to the model $\hat{H}_e^{\{0,L\},*}(s, \boldsymbol{\theta_{e,3}})$ by fixing the other two free parameters one at a time, for instance $\tau_{e,c}^{+} = 568.50$ s to evaluate both parameters $\tau_{e,c}^{-}$ and $\tau_{e,d}$ or $\tau_{e,c}^{-} = 379.00$ s to evaluate both parameters $\tau_{e,c}^{+}$ and $\tau_{e,d}$. These results are reported in Fig. 3c and Fig. 3d, respectively. Multiple parameter combinations $(\tau_{e,c}^{-}, \tau_{e,d})$ and $(\tau_{e,c}^{+}, \tau_{e,d})$ exhibit a valley in the cost function, whose minima are depicted as the dashed cyan curve. Just as before, these relationships seem to be nonlinear.

In order to attempt to solve the identifiability problem, we evaluated an electrolyte concentration equilibrium point different than eq1 specified above, now corresponding to $c_{e,0} = 10c_{e,\text{eq}}$ and $c_{e,L} = c_{e,\text{eq}}/10$ and it is denoted as eq2. This choice is arbitrary, and it implies the case where a given current signal is injected into the battery to form an electrolyte concentration gradient in steady-state between the negative and positive electrodes, or battery terminals at $x = 0$ and $x = L$, respectively[2]. Using this new condition, we repeated the experiments previously described and the parameter combinations that minimize the cost function (31) are shown in Fig. 3 as dotted magenta curves labelled with eq2. The different operating condition does not impact the results obtained with the simple model $\bar{H}_e^{\{0,L\},*}(s, \boldsymbol{\theta_{e,2}})$ (see Fig. 3a) but it does generate a different optimal parameter combination for model $\hat{H}_e^{\{0,L\},*}(s, \boldsymbol{\theta_{e,3}})$ (see Fig. 3b to Fig. 3d) with respect to eq1. Note how the two curves eq1 and eq2 intersect in the red point of nominal parameters. These results suggest that by changing the operating conditions, one could favor the estimation of a given group of parameters, hence alleviating the identifiability problem originally obtained for a given electrolyte impedance model.

V. CONCLUSIONS

Several impedance models for electrolyte dynamics in lithium-ion batteries were presented and their identifiability properties were analyzed. From these impedance responses, it was shown that simple models with two parameters and slightly more complex models with three parameters exhibit similar capacitive behaviour. The minimum number of parameters uniquely parameterising these models was characterised. However, it was also shown how these models suffered from structural identifiability issues, with different parameter values giving equivalent impedance responses. This insensitivity in the impedance responses will result in difficulty in correctly parameterising these models. It was also observed that these identifiability issues could be removed for non-symmetric cells by combining impedance measurements made around different steady-state operating points. Overall, this work highlights the importance of electrolyte model selection for expected system response and parameter identification. Future work seeks to determine model parameters from experimental data.

APPENDIX

The general electrolyte impedance models for positions $x = 0$ and $x = L$ are respectively given by (A.1) at the top of the page with $H_e^{\{0,L\},*}(s, \boldsymbol{\theta}) = C_e^{\{0,L\},*}(s)/I^*(s)$. In these expressions, $\tau_{e,c}^{\pm}$ are given by (10), $\beta^{i,j}$ with $i \in \{+, -, s\}$ and $j \in \{n, ns, \cdot\}$ are given by

$$\beta^{-,n} = \sqrt{\tau_{e,d}^{-,n} s}, \quad \beta^{s,n} = \sqrt{\tau_{e,d}^{s,n} s}, \quad \beta^{s,ns} = \sqrt{\tau_{e,d}^{s,ns} s},$$
$$\beta^{+,ns} = \sqrt{\tau_{e,d}^{+,ns} s}, \quad \beta^{+} = \sqrt{\tau_{e,d}^{+} s}, \tag{A.2}$$

[2]Enforcing an equilibrium with an electrolyte concentration gradient requires a non-zero current whose effects will be explored in future work.

$$H_{e,0}^{-,*}(s,\boldsymbol{\theta}) = \frac{(\tau_{e,c}^{-})^{-1}(\exp(\beta^{-,n})-1)^2\Sigma_1 + (\tau_{e,c}^{-})^{-1}(1-\exp(2\beta^{-,n}))\Sigma_2 - (\tau_{e,c}^{+})^{-1}4\rho^{+}\rho^{s}\sigma_5(\exp(2\beta^{+,ns})-\exp(2\beta^{+}))}{s\left((1+\exp(2\beta^{-,n}))\Sigma_1 + (1-\exp(2\beta^{-,n}))\Sigma_2\right)} \tag{A.1a}$$

$$H_{e,L}^{+,*}(s,\boldsymbol{\theta}) = \frac{-(\tau_{e,c}^{+})^{-1}(1+\exp(2\beta^{-,n}))\Sigma_3 - (\tau_{e,c}^{+})^{-1}(1-\exp(2\beta^{-,n}))\Sigma_4 + (\tau_{e,c}^{-})^{-1}4\rho^{-}\rho^{s}\sigma_7(1-\exp(2\beta^{-,n}))}{s\left((1+\exp(2\beta^{-,n}))\Sigma_1 + (1-\exp(2\beta^{-,n}))\Sigma_2\right)} \tag{A.1b}$$

the electrolyte diffusion time constants $\tau_{e,d}^{i,j}$ take the form

$$\begin{aligned} \tau_{e,d}^{-,n} &= \frac{\varepsilon_e^{-}L_n^2}{D_{e,\text{eff}}^{-}}, \quad \tau_{e,d}^{s,n} = \frac{\varepsilon_e^{s}L_n^2}{D_{e,\text{eff}}^{s}}, \quad \tau_{e,d}^{s,ns} = \frac{\varepsilon_e^{s}L_{ns}^2}{D_{e,\text{eff}}^{s}}, \\ \tau_{e,d}^{+,ns} &= \frac{\varepsilon_e^{+}L_{ns}^2}{D_{e,\text{eff}}^{+}}, \quad \tau_{e,d}^{+} = \frac{\varepsilon_e^{+}L^2}{D_{e,\text{eff}}^{+}}, \end{aligned} \tag{A.3}$$

the variables $\Sigma_{1:4}$ are given by

$$\begin{aligned} \Sigma_1 &= \rho^{s}\left[\rho^{s}(\sigma_1-\sigma_2+\sigma_3-\sigma_4)+\rho^{+}(-\sigma_1-\sigma_2+\sigma_3+\sigma_4)\right], \\ \Sigma_2 &= \rho^{-}\left[\rho^{s}(\sigma_1+\sigma_2+\sigma_3+\sigma_4)+\rho^{+}(-\sigma_1+\sigma_2+\sigma_3-\sigma_4)\right], \\ \Sigma_3 &= \rho^{s}[\rho^{s}(\sigma_3-\sigma_4+\sigma_1-\sigma_2-2\sigma_6\sigma_8)+\rho^{+}(-\sigma_1-\sigma_2+\sigma_3+\sigma_4)], \\ \Sigma_4 &= \rho^{-}[\rho^{s}(\sigma_1+\sigma_2+\sigma_3+\sigma_4-2\sigma_6\sigma_9)+\rho^{+}(-\sigma_1+\sigma_2+\sigma_3-\sigma_4)], \end{aligned} \tag{A.4}$$

the variables ρ^{i} are

$$\rho^{-} = \frac{D_{e,\text{eff}}^{-}}{L^2}, \quad \rho^{s} = \frac{D_{e,\text{eff}}^{s}}{L^2}, \quad \rho^{+} = \frac{D_{e,\text{eff}}^{+}}{L^2}, \tag{A.5}$$

and the variables $\sigma_{1:9}$ are

$$\begin{aligned} &\sigma_1 = \exp(2\beta^{s,n})\exp(2\beta^{+}), \quad \sigma_2 = \exp(2\beta^{s,ns})\exp(2\beta^{+}), \\ &\sigma_3 = \exp(2\beta^{s,n})\exp(2\beta^{+,ns}), \quad \sigma_4 = \exp(2\beta^{+,ns})\exp(2\beta^{s,ns}), \\ &\sigma_5 = \exp(\beta^{-,n})\exp(\beta^{s,n})\exp(\beta^{s,ns}), \quad \sigma_6 = \exp(\beta^{+})\exp(\beta^{+,ns}), \\ &\sigma_7 = \exp(\beta^{+})\exp(\beta^{+,ns})\exp(\beta^{s,ns})\exp(\beta^{s,n}), \\ &\sigma_8 = \exp(2\beta^{s,n})-\exp(2\beta^{s,ns}), \quad \sigma_9 = \exp(2\beta^{s,n})+\exp(2\beta^{s,ns}). \end{aligned} \tag{A.6}$$

REFERENCES

[1] C. Iclodean, B. Varga, N. Burnete, D. Cimerdean, and B. Jurchiş. Comparison of different battery types for electric vehicles. *IOP Conference Series: Materials Science and Engineering*, 252:012058, 2017.

[2] X. Hu, S. Li, and H. Peng. A comparative study of equivalent circuit models for Li-ion batteries. *Journal of Power Sources*, 198:359–367, 2012.

[3] J. Newman and K.E. Thomas-Alyea. *Electrochemical Systems*. John Wiley & Sons, Inc., Hoboken, New Jersey, 3rd edition edition, 2004.

[4] Gang Ning and Branko N. Popov. Cycle life modeling of lithium-ion batteries. *Journal of The Electrochemical Society*, 151(10):A1584–A1591, 2004.

[5] S. Santhanagopalan, Q. Guo, P. Ramadass, and R. E. White. Review of models for predicting the cycling performance of lithium ion batteries. *Journal of Power Sources*, 156(2):620–628, 2006.

[6] S. J. Moura, F. B. Argomedo, R. Klein, A. Mirtabatabaei, and M. Krstic. Battery state estimation for a single particle model with electrolyte dynamics. *IEEE Transactions on Control Systems Technology*, 25(2):453–468, 2017.

[7] E. Prada, D. Di Domenico, Y. Creff, J. Bernard, V. Sauvant-Moynot, and F. Huet. Simplified electrochemical and thermal model of LiFePO4-Graphite Li-ion batteries for fast charge applications. *Journal of The Electrochemical Society*, 159(9):A1508–A1519, 2012.

[8] J. Marcicki, M. Canova, A. T. Conlisk, and G. Rizzoni. Design and parametrization analysis of a reduced-order electrochemical model of Graphite/LiFePO4 cells for SOC/SOH estimation. *Journal of Power Sources*, 237:310–324, 2013.

[9] Saeed Khaleghi Rahimian, Sean Rayman, and Ralph E. White. Extension of physics-based single particle model for higher charge–discharge rates. *Journal of Power Sources*, 224(0):180–194, 2013.

[10] Tanvir R. Tanim, Christopher D. Rahn, and Chao-Yang Wang. State of charge estimation of a lithium ion cell based on a temperature dependent and electrolyte enhanced single particle model. *Energy*, 80:731–739, 2015.

[11] Scott G. Marquis, Valentin Sulzer, Robert Timms, Colin P. Please, and S. Jon Chapman. An asymptotic derivation of a single particle model with electrolyte. *Journal of Power Sources*, 2019.

[12] Godfrey Sikha and Ralph E. White. Analytical expression for the impedance response of an insertion electrode cell. *Journal of The Electrochemical Society*, 154(1):A43–A54, 2007.

[13] A. M. Bizeray, J. Kim, S. R. Duncan, and D. A. Howey. Identifiability and parameter estimation of the single particle lithium-ion battery model. *IEEE Transactions on Control Systems Technology*, 27(5):1862 – 1877, 2019.

[14] Ross Drummond and Stephen R Duncan. Structural identifiability of a pseudo-2D Li-ion battery electrochemical model. *IFAC-PapersOnLine*, 53(2):12452–12458, 2020.

[15] Dong Zhang, Luis D Couto, and Scott J Moura. Electrode-level state estimation in lithium-ion batteries via Kalman decomposition. *IEEE Control Systems Letters*, 5(5):1657–1662, 2020.

[16] L. Ljung. *System identification, theory for the user*. Prentice Hall PTR, Upper Saddle River, New Jersey, 2nd edition edition, 1999.

[17] S. M. M. Alavi, A. Mahdi, S. J. Payne, and D. A. Howey. Identifiability of generalized Randles circuit models. *IEEE Transactions on Control Systems Technology*, 25(6):2112–2120, 2017.

[18] Uwe Westerhoff, Kerstin Kurbach, Frank Lienesch, and Michael Kurrat. Analysis of lithium-ion battery models based on electrochemical impedance spectroscopy. *Energy Technology*, 4(12):1620–1630, 2016.

[19] Woosung Choi, Heon-Cheol Shin, Ji Man Kim, Jae-Young Choi, and Won-Sub Yoon. Modeling and applications of electrochemical impedance spectroscopy (EIS) for lithium-ion batteries. *J. Electrochem. Sci. Technol*, 11(1):1–13, 2020.